AIMS Mathematics, 10(12): 29498–29521.
DOI: 10.3934/math.20251296
Received: 11 October 2025
Revised: 01 December 2025
Accepted: 03 December 2025
Published: 15 December 2025

https://www.aimspress.com/journal/Math

Research article

Dynamics and interaction of optical solitons in the nonlinear paraxial wave equation with sensitivity analysis

Meshari Alesemi*

Department of Mathematics, College of Science, University of Bisha, P.O. Box 511, Bisha 61922, Saudi Arabia

* **Correspondence:** Email: malesemi@ub.edu.sa.

Abstract: This research study explores novel multitude of optical soliton solutions of the (2 + 1)-dimensional nonlinear paraxial wave equation by three ansatzes, namely the generalised Kudryashov-auxiliary method, tan-cot method, and tanh-coth method. The model under consideration is particularly applied to the study of the wave propagation in nonlinear materials such as Kerr media. Using the simulation tool Maple, we compute breather and other optical soliton solutions in the forms of Jacobian elliptic, hyperbolic, periodic breather, breather-interaction, dark and bright solutions for the selected nonlinear paraxial wave equation with the aid of the suggested techniques. We also provide a series of two- and three-dimensional plots that represent the dynamics and interaction of the identified optical soliton solutions by assigning numerical values to the involved free parameters. We also carry out dynamical analysis to determine the stability of the model to the variation in the parameters and initial conditions and to gain a clearer understanding of how the system is prone to chaos. The obtained outcomes are very vital in fiber optics, nonlinear optics, and communication systems. Finally, the techniques used provide clear-cut soliton solutions of nonlinear partial differential equations, which can enhance the study of nonlinear wave phenomena and provide new insights into the dynamics of other complex systems.

Keywords: nonlinear paraxial wave equation; analytical methods; breather soliton; Kerr media; Hamiltonian analysis
Mathematics Subject Classification: 34G20, 35A20, 35A22, 35R11

1. Introduction

Numerous scientific fields, including geochemistry, physics, engineering, biology, plasma physics, economics, and cosmology employ nonlinear partial differential equations (NPDEs) to depict intricate phenomena. Linear equations do not accurately capture nonlinear interdependence and interactions.

Studying nonlinear systems such as pattern generation, fluid dynamics, nonlinear optics, and response diffusion processes are made easier with the help of NPDEs [1–4]. These equations require special methods to get their solutions due to their significance and applicability. A complex-structured NPDE is a basic mathematical concept with numerous applications in engineering, science and daily life [5–7]. These formulas offer a comprehensive mathematical framework that explains the intricate relationships between large systems with both imaginary and real parts [8–10]. The fundamental features of such NPDEs, which may represent nonlinear phenomena, are investigated using solitonic solutions found in a variety of fields, including electrical circuits, solid state, plasma physics, fluid dynamics, and bioscience, among others [11–13]. Numerous academics have been interested in studying solitons, and they have been linked to a number of characteristics of solitary wave solutions [14–16]. These soliton solutions can be generated analytically by applying methods like the Darboux transform method [17], the Hirota method [18], the extended trial equation technique [19], the inverse scattering transform method [20], the Riccati modified simple equation method [21], the Jacobi elliptic function method [22], the Exp-function method [23], the Kudryashov method [24], the generalised Kudryashov-Auxiliary Method (GKAM) [25], the sine-cosine method [26], the first integral method [27], the tanh-coth method [28], the soliton ansatz technique [29], the direct algebraic method [30], the tan-cot method [31], the Khater method [32], the extended tanh function method [33], the unified method [34], and the (G'/G)-expansion method [35].

Among the complex-structured NPDEs, the nonlinear paraxial wave equation (NPWE) is a mathematical model used in photonics and optics that is especially helpful for researching wave propagation in nonlinear materials such as Kerr media. Understanding nonlinear optical processes requires an understanding of the NPWE, particularly in Kerr media where refractive index is influenced by light intensity [36]. In biomedical imaging methods such as optical coherence tomography and multiphoton microscopy, the NPWE improves imaging resolution through nonlinear effects and helps comprehend light-tissue interactions [37]. This model is mathematically represented as [38]:

$$iz_y + \frac{\mu}{2}z_{xx} + \frac{\lambda}{2}z_{tt} - \nu z|z|^2 = 0, \tag{1.1}$$

where $z = z(x, y, t)$ is a complex-valued function that represents wave profile, the dispersion impact is denoted by λ, the diffraction effect by μ and the Kerr non-linearity effect by ν, such that $\lambda, \mu, \nu \in R$. In this equation, the first term denotes phase evolution; the second term, $\frac{\mu}{2}z_{xx}$, represents transverse diffraction; the third term, $\frac{\lambda}{2}z_{tt}$, governs temporal compression or broadening of pulses; and the Kerr-type cubic nonlinear term, $\nu z|z|^2$, represents intensity-dependent refractive index changes, respectively. In order to focus on the parametric wave condition in a Kerr medium, Baronio [39] adopted the one-layered dissipation limit while taking time-subordinate space-time and bunch speed scattering into account. The NPWE is also known as a ray equation which offers a condensed approximation of the full wave equation [40] for the purpose of simulating light propagation in a material. Many other researchers have addressed the proposed model in both fractional and integer sense with different analytical tools for soliton solutions. For example, Bashar et al. used the extended auxiliary mapping method to examine the bright and dark, periodic, bell-shaped, and singular-type optical soliton solutions of the truncated time M-fractional NPWE [38]. Younas et al. analyzed diversity of solitary wave structures in the context of complex NPWEs in Kerr media [41]. Saad explored breather, lump, rogue wave, and interaction solutions to the fractional NPWE using the

Sardar sub-equation method and the Hirota bilinear method with sensitivity analysis of the model [42]. Finally, Wang and Wei used the functional variable method, the Sine-Gordon expansion method, and the Bernoulli (G'/G)-expansion method to establish novel optical soliton solutions for the NPWE [43]. Nevertheless, no work has constructed optical soliton solutions for the NPWE with dynamical analysis of the model via phase portraits and time series plots using the suggested GKAM, tan-cot technique, and tanh-coth method. This assertion highlights a significant gap in the body of current research. Our research fills this gap by adopting the suggested methods and offering a thorough model analysis.

The main aim of this investigation is to study the characteristic optical solutions of the NPWE with the use of three ansatzes, namely GKAM, tan-cot method, and tanh-coth method. In the context of the NPWE, we find breather and other optical solitons solutions in the forms of Jacobian elliptic, hyperbolic, and trigonometric functions by the methods proposed. These solutions consist of smooth breather, singular breather, periodic breather, breather-interaction, and dark and bright solutions. We also provide a set of two- and three-dimensional plots that depict the dynamics and interaction of the discovered optical soliton solutions for the numerical value of the free parameters. To more clearly see how the system is sensitive to perturbation, we also perform dynamical analysis to observe the flexibility the chosen model against the variations of the parameters and initial conditions. The obtained results are important to the fiber optics, nonlinear optics, and communication systems.

The following sections are structured as follows: Section 2 presents the governing equation, constraint condition, and dynamical analysis of the model; Section 3 offers the working mechanisms of the proposed methods; Section 4 addresses the proposed model with the proposed model to produce novel optical soliton solutions for the NPWE; Section 5 provides and discusses the numerical simulations and graphical representations of some of the obtained results; and Section 6 provides novelties, comparative analysis, and limitations of the study. Subsequently, the article concludes with a summary of its findings and future goals.

2. The governing equation

In order to get the governing equation, we transform NPDE of the model given as:

$$iz_y + \frac{\mu}{2}z_{xx} + \frac{\lambda}{2}z_{tt} - \nu z|z|^2 = 0, \tag{2.1}$$

into a more manageable nonlinear ordinary differential equation (NODE) through the establishment of the following complex structured wave transformation:

$$z(x, y, t) = Z(\varpi)e^{i\Xi}, \quad \varpi = ax + by + ct, \quad \Xi = mx + ny + pt + q, \tag{2.2}$$

where a, b, c, m, n, and p are wave numbers, and q is a phase component. When incorporated in (2.2), this transformation extracts the ensuing governing NODE from the real part:

$$\left(\mu a^2 + \lambda c^2\right)Z''(\varpi) - \left(\lambda p^2 + \mu m^2 + 2n\right)Z(\varpi) - 2\nu\,(Z(\varpi))^3 = 0, \tag{2.3}$$

while the imaginary part provides:

$$2(b + am\mu + c\lambda p)Z'(\varpi) = 0. \tag{2.4}$$

Because $Z'(\varpi) \neq 0$, we get the following constraint condition from (2.4):

$$b = -am\mu - c\lambda p.$$

2.1. Analysis of the governing model

The present section provides analysis of the governing model through Hamiltonian analysis, phase portraits, and time-series plots. The planner system of the model can be obtained from the (2.3) as:

$$\begin{aligned} F(Z,S) &= Z' = S, \\ G(Z,S) &= S' = MZ + NZ^3, \end{aligned} \tag{2.5}$$

while the perturbed system (when an external periodic term is added to the second component in (2.5)) of the model can be obtained as:

$$\begin{aligned} F(Z,S) &= Z' = S, \\ L(Z,S) &= S' = MZ + NZ^3 + h_0 \sin(h_1 \varpi), \end{aligned} \tag{2.6}$$

where h_0 and h_1 are constants and

$$M = \frac{\lambda\, p^2 + m^2\mu + 2\,n}{a^2\mu + c^2\lambda}, \quad N = 2\,\frac{\nu}{a^2\mu + c^2\lambda}.$$

To get the Hamiltonian of the system, we write the planner system represented by (2.5) in canonical form given by

$$\begin{aligned} \frac{\partial H(Z,S)}{\partial S} &= Z' = S, \\ \frac{\partial H(Z,S)}{\partial Z} &= -S' = -MZ - NZ^3. \end{aligned} \tag{2.7}$$

By integrating with respect to S once, the first equation in (2.7) gives $H(Z,S) = \frac{S^2}{2} + f(Z)$, which implies $\frac{\partial H(Z,S)}{\partial Z} = \frac{\partial f(Z)}{\partial Z}$. But by the second equation of (2.7), $\frac{\partial H(Z,S)}{\partial Z} = -MZ - NZ^3$ thus $\frac{\partial f(Z)}{\partial Z} = -MZ - NZ^3$, which by integration implies $f(Z) = -M\frac{Z^2}{2} - N\frac{Z^4}{4}$. Subsequently, we get the following canonical Hamiltonian with a constant for the system:

$$H(Z,S) = \frac{S^2}{2} - M\frac{Z^2}{2} - N\frac{Z^4}{4} = constant. \tag{2.8}$$

Under this Hamiltonian, we get three equilibria along the Z-axis: $(P_0, 0) = (0, 0)$ and $(P_\pm, 0)$, where $P_\pm$ is given as

$$P_\pm = \pm\sqrt{-\frac{\lambda\, p^2 + m^2\mu + 2\,n}{2\nu}}. \tag{2.9}$$

Moreover, by the Jacobian matrix;

$$J = \begin{bmatrix} \frac{\partial F}{\partial Z} & \frac{\partial F}{\partial S} \\ \frac{\partial G}{\partial S} & \frac{\partial G}{\partial S} \end{bmatrix}, \tag{2.10}$$

we get the following Jacobian;

$$|J(Z,S)| = -M - 3NZ^2. \tag{2.11}$$

Because the system is Hamiltonian, equilibria are either centers (elliptic) or saddles (hyperbolic), and hence no repelling and attracting foci or nodes occur. To find the nature of equilibria, we estimate the eigenvalues of the Jacobian matrix at the three different equilibrium points as follows:

i. At $(P_0, 0)$, we have

$$J(P_0) = \begin{bmatrix} 0 & 1 \\ M & 0 \end{bmatrix}, \tag{2.12}$$

which implies

$$\lambda_{\pm} = \pm\sqrt{M}. \tag{2.13}$$

Thus, we conclude that the point $(0, 0)$ is center if $M < 0$ (because the eigenvalues $\lambda_{\pm}$ are real) , saddle if $M > 0$ (because the eigenvalues $\lambda_{\pm}$ are pure imaginary), and hyperbolic/degenerate if $M = 0$, which requires higher order analysis.

ii. At $(P_{\pm}, 0)$, we have

$$J(P_{\pm}) = \begin{bmatrix} 0 & 1 \\ -2M & 0 \end{bmatrix}, \tag{2.14}$$

which implies

$$\lambda_{\pm} = \pm\sqrt{-2M}. \tag{2.15}$$

Thus, we conclude that the point $(P_{\pm}, 0)$ is center if $M > 0$ (because the eigenvalues $\lambda_{\pm}$ are real), saddle if $M < 0$ (because the eigenvalues $\lambda_{\pm}$ are pure imaginary), and degenerate if $M = 0$, which requires higher order analysis. With the presence of Hamiltonian constant, we now investigate the bifurcations of phase portraits in the parameter space M and N for (2.5) and (2.6).

2.1.1. The bifurcation of phase portraits

By assigning arbitrary values to the involved parameters, we first present some phase portraits for both planner and perturbed systems presented in (2.5) and (2.6) respectively.

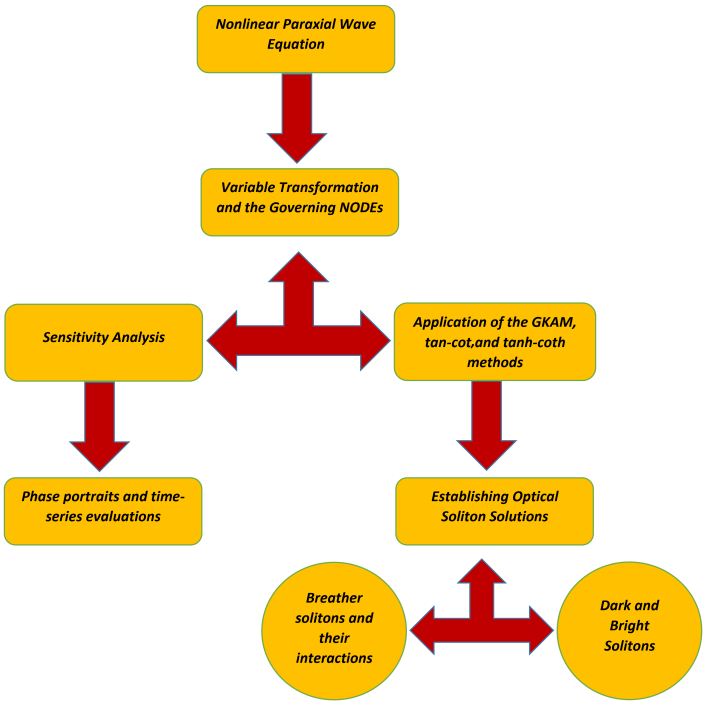

Figure 1. The layout of the current research study.

The Figure 1, shows the flowchart of the methodology. In Figure 2, the phasDe portraits represent families of closed orbits with a single center at $(0, 0)$ surrounded by circular smooth trajectories, which reveal regular periodic dynamics.

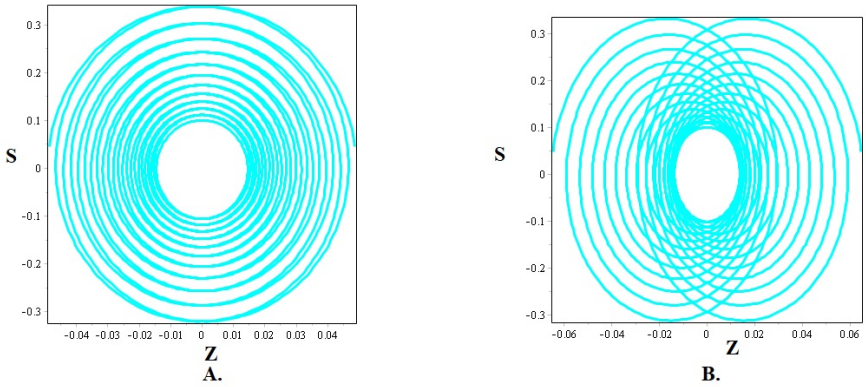

Figure 2. Phase portraits of **A.** Planner system presented in (2.5) and **B.** Perturbed system presented in (2.6) for $a = 0.1, c = 0.1, \lambda = 0.1, \mu = 0.1, \nu = 0.05, m = 0.02, n = -0.05, p = 0.05, h_0 = 1$, and $h_1 = 0.1$ and considering the initial conditions $Z(0) = 0, S(0) = 0.1$, respectively.

In Figure 3, the phase portraits represent closed loops centered at $(0, 0)$, which again reveal classical periodic motion. Figure 4, represents homoclinic orbits with two smooth and symmetric centers at $(0.775, 0)$ and $(-0.775, 0)$ and a saddle point at $(0, 0)$ through which the separatrix loops pass. The trajectories inside each lobe are round and periodic. Based on the phase portraits, the system is not chaotic.

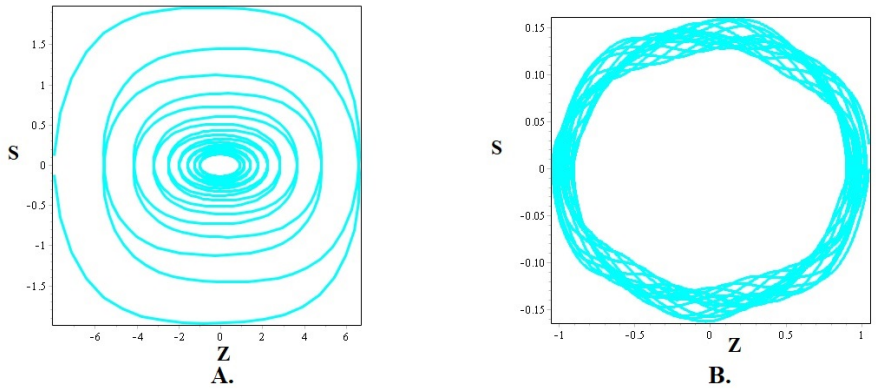

Figure 3. Phase portraits of **A.** Planner system presented in (2.5) and **B.** Perturbed system presented in (2.6) for $a = 5, c = 5, \lambda = 1, \mu = 1, \nu = -0.05, m = -0.03, n = -1, p = -1, h_0 = 0.01$, and $h_1 = 1$ and considering the initial conditions $Z(0) = 0.9, S(0) = 0$, respectively.

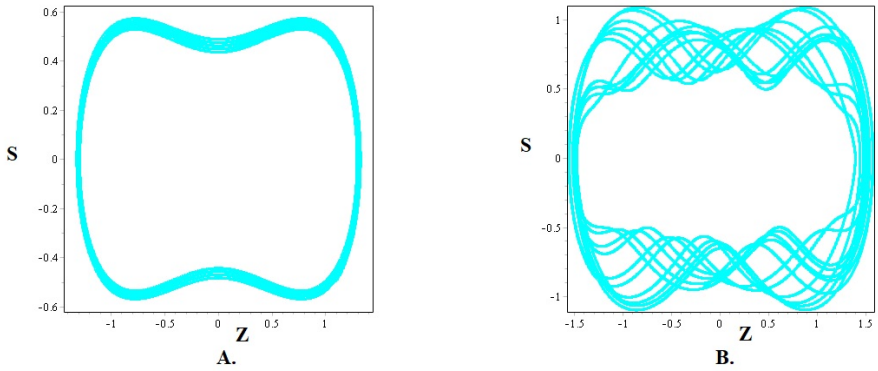

Figure 4. Phase portraits of **A.** Planner system presented in (2.5) and **B.** Perturbed system presented in (2.6) for $a = 1, c = 1, \lambda = 1, \mu = 1, \nu = -0.5, m = 0, n = -0.2, p = 1, h_0 = 0.6$, and $h_1 = 3$ and considering the initial conditions $Z(0) = 0.5, S(0) = 0.5$, respectively.

2.1.2. Time-series plots

We now present some time-series plots (temporal traceries that show the evolving nature of a model's underlying mechanism) for the perturbed system presented in (2.6). These plots are drawn for different initial conditions and by assigning arbitrary values to the involved parameters.

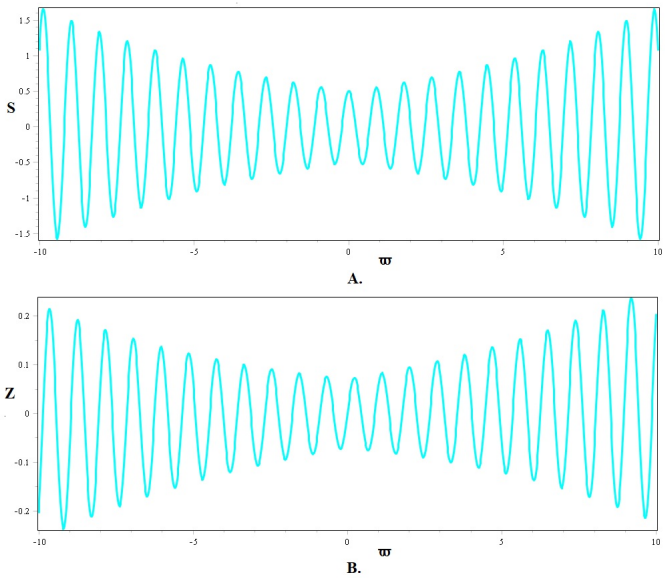

Figure 5. Time-series plots of **A.** $S(\varpi)$ and **B.** $Z(\varpi)$ presented by (2.6) for $a = 0.1, c = 0.1, \lambda = 0.1, \mu = 0.1, \nu = 0.05, m = 0.02, n = -0.05, p = 0.05, h_0 = 1$, and $h_1 = 0.1$ and considering the initial conditions $Z(0) = 0, S(0) = 0.5$.

Altogether, we obtained periodic (signals having periodicity in amplitudes), quasi-periodic (two or multiple incompatible wavelengths superimposed), and fractal-like periodic (patterns displaying similarities and scaling tendencies over periods of time while having a dominating periodic structure) type time-series plots for the perturbed system. In Figure 5, the time-series plots are quasi-periodic, as

the motion does not repeat exactly but remains smooth and bounded. This quasi-periodicity suggests no chaos in the system.

In Figure 6, the time-series plots are periodic, which confirms that the system is periodic with stable oscillations. Finally, the time-series plots in Figure 7, reveal fractal-like periodic and quasi-periodic trajectories. The trajectories are bounded and organized, which indicates that system is weakly chaotic. Based on these time-series plots, we conclude that the system is periodic and not not fully chaotic.

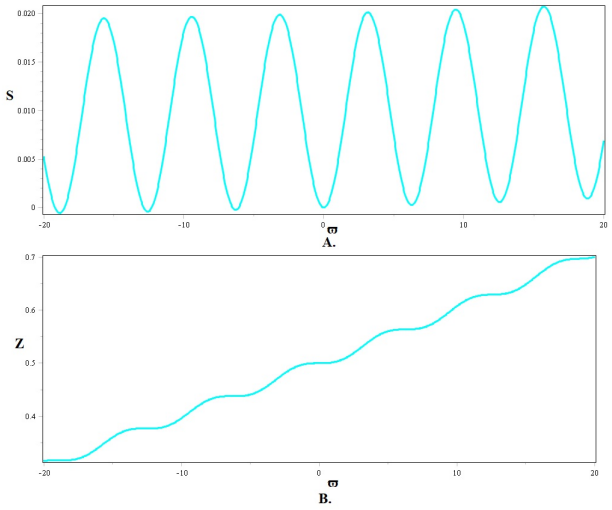

Figure 6. Time-series plots of **A.** $S(\varpi)$ and **B.** $Z(\varpi)$ presented by (2.6) for $a = 100, c = 100, \lambda = 1, \mu = 1, \nu = 0.5, m = 0.3, n = 0.1, p = 1, h_0 = 0.01$, and $h_1 = 1$ and considering the initial conditions $Z(0) = 0.5, S(0) = 0$.

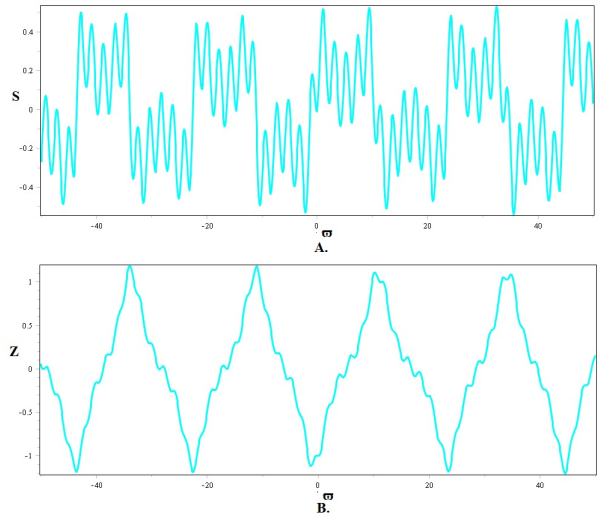

Figure 7. Time-series plots of **A.** $S(\varpi)$ and **B.** $Z(\varpi)$ presented by (2.6) for $a = 1, c = 1, \lambda = 1, \mu = 1, \nu = -0.5, m = 0, n = -0.2, p = 1, h_0 = 0.6$, and $h_1 = 3$ and considering the initial conditions $Z(0) = -1, S(0) = 0$.

3. Presentations of proposed methods

This section provides the layouts of the used methods. Take into account the following general NPDE:

$$A(z, z_t, z_{\zeta_1}, |z_{\zeta_1}|, z_{\zeta_2}, zz_{\zeta_1}, z|z|, ...) = 0, \tag{3.1}$$

where $z = z(t, \zeta_1, \zeta_2, \zeta_3, ..., \zeta_l)$. To deal with (3.1), the subsequent steps are to be performed:

Step 1. A complex variable transformation is firstly applied to (3.1) of the structure $z(t, \zeta_1, \zeta_2, \zeta_3, ..., \zeta_n) = e^{i\Xi}Z(\varpi)$, where $\varpi = \varpi(t, \zeta_1, \zeta_2, \zeta_3, ...\zeta_l)$ and $\Xi = \Xi(t, \zeta_1, \zeta_2, \zeta_3, ...\zeta_l)$. As a result of this transformation, we get a nonlinear ordinary differential equation (NODE) from (3.2) of the form

$$B(Z, Z', ZZ', \dots) = 0, \tag{3.2}$$

where the derivatives of ϖ are shown by the primes in (3.2). To satisfy homogeneous balance requirements, (3.2) is seldom integrated once or more.

3.1. The operational mechanism of GKAM

We start by outlining GKAM's operational mechanism. To address (3.2), we undertake the procedures mentioned in [25].

Step 2. The essential premise of the GKAM is that the closed form solution for (3.2) may be expressed as follows:

$$Z(\varpi) = \sum_{r=-\Omega}^{\Omega} \frac{\eta_r}{(1 + G(\varpi))^r}, \tag{3.3}$$

where the parameters that require estimation are indicated by $\eta_r's; (r = -\Omega, ..., \Omega)$. Additionally, the following NODE is satisfied by $G(\varpi)$:

$$G'(\varpi) = \sqrt{\rho + \varrho G^2(\varpi) + \sigma G^4(\varpi)}, \tag{3.4}$$

where the constants ρ, ϱ, and σ are used, and the solution $G(\varpi)$ corresponds to Jacobian elliptic functions that change according to the particular values given to ρ, ϱ, and σ.

Step 3. The positive integer Ω, which is displayed in (3.3), is obtained when we set for the homogeneous balancing criteria between the main nonlinear term and greatest order derivative in (3.2).

Step 4. A polynomial of $G(\varpi)$ with different powers is then obtained by putting (3.3) in (3.2) and its associated derivatives based on (3.4). An algebraic equation system for η_r's and other parameters is obtained when all of the coefficients of this polynomial are equal to zero. A symbolic computation tool Maple is then used to solve the resultant set of nonlinear algebraic equations.

Step 5. The precise soliton solutions to (3.1) are obtained using equation (3.3), the related solution $G(\varpi)$ from (3.4), and the computed parameters. The varieties of soliton solutions produced by running the general solution of (3.4) are displayed in Table 1.

Table 1. The types of Jacobian elliptic solutions $G(\varpi)$ of (3.4).

Types	ρ	ϱ	σ	**Solutions**
1.1	$1-s^2$	$2-s^2$	1	$cs(\varpi)$
1.2	$\frac{1}{4}$	$\frac{1-2s^2}{2}$	$\frac{1}{4}$	$ns(\varpi) \pm cs(\varpi)$, $\frac{sn(\varpi)}{1\pm cn(\varpi)}$
1.3	$\frac{1-s^2}{4}$	$\frac{1+s^2}{2}$	$\frac{1-s^2}{4}$	$nc(\varpi) + sc(\varpi)$
1.4	1	$2-s^2$	$1-s^2$	$sc(\varpi)$
1.5	1	$2s^2-1$	$-s(1-s^2)$	$sd(\varpi)$
1.6	1	$2-4s^2$	1	$\frac{sn(\varpi)dn(\varpi)}{cn(\varpi)}$
1.7	1	2	s^2	$\frac{sn(\varpi)cn(\varpi)}{dn(\varpi)}$

The subsequent transformation illustrates how the parameter s separates the solutions of (3.4) into hyperbolic and trigonometric functions; that is, as the parameter s gets closer to 1, the solutions involving Jacobian elliptic functions change into hypergeometric functions:

$$\{ds(\varpi), cs(\varpi)\} \to csch(\varpi), \{cn(\varpi), dn(\varpi)\} \to sech(\varpi),\ sn(\varpi) \to \tanh(\varpi),$$
$$\{nc(\varpi), nd(\varpi)\} \to \cosh(\varpi), \{sc(\varpi), sd(\varpi)\} \to \sinh(\varpi),\ ns(\varpi) \to \coth(\varpi),\ \{cd(\varpi), dc(\varpi)\} \to 1.$$

Likewise, when the parameter s gets closer to zero, the transformation of the Jacobian elliptic function solutions yields the following trigonometric functions:

$$\{cn(\varpi), cd(\varpi)\} \to \cos(\varpi), sc(\varpi) \to \tan(\varpi),\ \{sn(\varpi), sd(\varpi)\} \to \sin(\varpi),$$
$$\{nc(\varpi), dc(\varpi)\} \to \sec(\varpi), \{ns(\varpi), ds(\varpi)\} \to \csc(\varpi),\ \{dn(\varpi), nd(\varpi)\} \to 1,\ cs(\varpi) \to \cot(\varpi).$$

3.2. The operational mechanism of tan-cot method

The tan-cot method [31] suggests the following closed form solution for the resulting NODE given in (3.3) in order to cope with (3.1):

$$Z(\varpi) = \sum_{r=-\Omega}^{\Omega} \eta_r \left(\tan(\varpi)\right)^r. \tag{3.5}$$

Equation (3.5) is substituted into Eq (3.3), or the equation that results from integrating equation (3.3) and combining the terms with the equivalent exponents of $\tan^k(\varpi)$, using the calculated value of the balance number Ω to produce an expression in terms of $\tan^k(\varpi)$ for some $k \in Z$. By matching the coefficients on both sides of the expression, an algebraic set of equations with the parameters $\eta_r; (r = -\Omega, ..., \Omega)$ and other associated parameters is produced. The algebraic program Maple is used to solve the resultant algebraic system and get the values of $\eta_r; (r = -\Omega, ..., \Omega)$ and other pertinent parameters. By changing the values of the parameters in Eq (3.5), one may find the solutions to Eq (3.1).

3.3. The operational mechanism of tanh-coth method

The tanh-coth method [28] suggests the following closed form solution for the resulting NODE given in (3.3) in order to cope with (3.1):

$$Z(\varpi) = \sum_{r=-\Omega}^{\Omega} \eta_r \left(\tanh(\varpi)\right)^r . \tag{3.6}$$

Equation (3.6) is substituted into Eq (3.3), or the equation that results from integrating equation (3.3) and combining the terms with the identical exponents of $\tanh(\varpi)$, using the calculated value of the balance number Ω to produce an expression in terms of $\tanh^k(\varpi)$ for some $k \in Z$. By comparing the coefficients on both sides of the expression, an algebraic set of equations with the parameters $\eta_r; (r = -\Omega, ..., \Omega)$ and other associated parameters is produced. The algebraic program Maple is used to solve the resultant algebraic system and get the values of $\eta_r; (r = -\Omega, ..., \Omega)$ and other pertinent parameters. By changing the values of the parameters in Eq (3.6), one may find the solutions to Eq (3.1).

4. Results

This section aims to establish solton solutions for the aimed model. Balancing $Z''(\varpi)$ with $Z^3(\varpi)$ presented in (2.3) implies $\Omega + 2 = 3\Omega$; thus, we get balance number $\Omega = 1$ defined in Step 3.

4.1. The application of GKAM

We firstly apply GKAM to (2.3) in order to provide novel soliton solutions for (2.1). The proposed GKAM presents the following close-form solution for (2.3) when $\Omega = 1$ is substituted in (3.3):

$$Z(\varpi) = \sum_{r=-1}^{1} \frac{\eta_r}{(1 + G(\varpi))^r}. \tag{4.1}$$

When incorporated in (2.3), this solution further converts the NODE into an expression in $G(\varpi)$. By collecting and equating the coefficients with the same powers of $G(\varpi)$ to zero, we get a system of algebraic equations. By inputting the resultant system into computational tool Maple, we get the following case of solutions for the system:

Case. A.1

$$\begin{aligned} &\eta_0 = -\eta_{-1}, \eta_1 = 0, \eta_{-1} = \eta_{-1}, a = a, c = c, m = m, q = q, \lambda = \lambda, \\ &n = \frac{1}{2} a^2 \mu \varrho + \frac{1}{2} c^2 \lambda \varrho - \frac{1}{2} \lambda p^2 - \frac{1}{2} m^2 \mu, \mu = \mu, \nu = \frac{\sigma \left(a^2 \mu + c^2 \lambda\right)}{{\eta_{-1}}^2}. \end{aligned} \tag{4.2}$$

By taking into account **Case. A.1** and utilizing (2.2) and (4.1) in addition to the replicating solution of (3.4), we yield the ensuing novel soliton solutions for (2.1):

Family. A.1: When $s \to 1$:

Subfamily. A.1.1: Taking $\rho = 1 - s^2$, $\varrho = 2 - s^2$, and $\sigma = 1$:

$$z_{A,1,1}(x, y, t) = \left(\eta_{-1} \operatorname{csch}(\varpi)\right) e^{i\Xi}. \tag{4.3}$$

Subfamily. A.1.2: Taking $\rho = \frac{1}{4}$, $\varrho = \frac{1-2s^2}{2}$, and $\sigma = \frac{1}{4}$:

$$z_{A,1,2}(x, y, t) = \left(\eta_{-1} \left(\coth(\varpi) \pm (\operatorname{csch}(\varpi))\right)\right) e^{i\Xi}, \tag{4.4}$$

and

$$z_{A,1,3}(x,y,t) = \left(\frac{\eta_{-1}\tanh(\varpi)}{1 \pm (\operatorname{sech}(\varpi))}\right)e^{i\Xi}. \tag{4.5}$$

Subfamily. A.1.3: Taking $\rho = \frac{1-s^2}{4}$, $\varrho = \frac{1+s^2}{2}$, and $\sigma = \frac{1-s^2}{4}$:

$$z_{A,1,4}(x,y,t) = \left(\eta_{-1}\left(\cosh(\varpi) + \sinh(\varpi)\right)\right)e^{i\Xi}. \tag{4.6}$$

Subfamily. A.1.4: Taking $\rho = 1$, $\varrho = 2 - s^2$, and $\sigma = 1 - s^2$:

$$z_{A,1,5}(x,y,t) = \left(\eta_{-1}\sinh(\varpi)\right)e^{i\Xi}. \tag{4.7}$$

Subfamily. A.1.5: Taking $\rho = 1$, $\varrho = 2s^2 - 1$, and $\sigma = -s(1 - s^2)$:

$$z_{A,1,6}(x,y,t) = \left(\eta_{-1}\sinh(\varpi)\right)e^{i\Xi}. \tag{4.8}$$

Subfamily. A.1.6: Taking $\rho = 1$, $\varrho = 2 - 4s^2$, and $\sigma = 1$:

$$z_{A,1,7}(x,y,t) = \left(\eta_{-1}\tanh(\varpi)\right)e^{i\Xi}. \tag{4.9}$$

Subfamily. A.1.7: Taking $\rho = 1$, $\varrho = 2$, and $\sigma = s^2$:

$$z_{A,1,8}(x,y,t) = \left(\eta_{-1}\tanh(\varpi)\right)e^{i\Xi}. \tag{4.10}$$

Family. A.2: When $s \to 0$:
Subfamily. A.2.1: Taking $\rho = 1 - s^2$, $\varrho = 2 - s^2$, and $\sigma = 1$:

$$z_{A,2,1}(x,y,t) = \left(\eta_{-1}\cot(\varpi)\right)e^{i\Xi}. \tag{4.11}$$

Subfamily. A.2.2: Taking $\rho = \frac{1}{4}$, $\varrho = \frac{1-2s^2}{2}$, and $\sigma = \frac{1}{4}$:

$$z_{A,2,2}(x,y,t) = \left(\eta_{-1}\left(\csc(\varpi) \pm (\cot(\varpi))\right)\right)e^{i\Xi}, \tag{4.12}$$

and

$$z_{A,2,3}(x,y,t) = \left(\frac{\eta_{-1}\sin(\varpi)}{1 \pm (\cos(\varpi))}\right)e^{i\Xi}. \tag{4.13}$$

Subfamily. A.2.3: Taking $\rho = \frac{1-s^2}{4}$, $\varrho = \frac{1+s^2}{2}$, and $\sigma = \frac{1-s^2}{4}$:

$$z_{A,2,4}(x,y,t) = \left(\eta_{-1}\left(\sec(\varpi) + \tan(\varpi)\right)\right)e^{i\Xi}. \tag{4.14}$$

Subfamily. A.2.4: Taking $\rho = 1$, $\varrho = 2 - s^2$, and $\sigma = 1 - s^2$:

$$z_{A,2,5}(x,y,t) = \left(\eta_{-1}\tan(\varpi)\right)e^{i\Xi}. \tag{4.15}$$

Subfamily. A.2.5: Taking $\rho = 1$, $\varrho = 2s^2 - 1$, and $\sigma = -s(1 - s^2)$:

$$z_{A,2,6}(x, y, t) = \left(\eta_{-1} \sin(\varpi)\right) e^{i\Xi}. \tag{4.16}$$

Subfamily. A.2.6: Taking $\rho = 1$, $\varrho = 2 - 4s^2$, and $\sigma = 1$:

$$z_{A,2,7}(x, y, t) = \left(\eta_{-1} \tan(\varpi)\right) e^{i\Xi}. \tag{4.17}$$

Subfamily. A.2.7: Taking $\rho = 1$, $\varrho = 2$, and $\sigma = s^2$:

$$z_{A,2,8}(x, y, t) = \left(\eta_{-1} \sin(\varpi) \cos(\varpi)\right) e^{i\Xi}, \tag{4.18}$$

where $\varpi = ax - (am\mu + c\lambda\, p)y + ct, \quad \Xi = mx + (\frac{1}{2}\, a^2\mu\, \varrho + \frac{1}{2}\, c^2\lambda\, \varrho - \frac{1}{2}\, \lambda\, p^2 - \frac{1}{2}\, m^2\mu)y + pt + q.$

4.2. The Application of tan-cot method

We now apply the tan-cot method to (2.3) in order to provide novel soliton solutions for (2.1). The proposed tan-cot method presents the following close-form solution for (2.3) when $\Omega = 1$ is substituted in (3.5):

$$Z(\varpi) = \sum_{r=-1}^{1} \eta_r \left(\tan(\varpi)\right)^r. \tag{4.19}$$

When incorporated in (2.3), this solution further converts the NODE into an expression in $\tan(\varpi)$. By collecting and equating the coefficients with the same powers of $\tan(\varpi)$ to zero, we get a system of algebraic equations. By running the resulting system through computational tool Maple, we get the following cases of solutions for the system:

Case. B.1

$$\begin{aligned} &\eta_0 = 0, \eta_1 = 0, \eta_{-1} = \eta_{-1}, a = a, c = c, m = m, q = q, \lambda = \lambda, \\ &n = a^2\mu + c^2\lambda - \frac{1}{2}\, \lambda\, p^2 - \frac{1}{2}\, m^2\mu, \mu = \mu, \nu = \frac{a^2\mu + c^2\lambda}{{\eta_{-1}}^2}. \end{aligned} \tag{4.20}$$

Which yields the following soliton solution:

$$z_{B,1,1}(x, y, t) = \left(\frac{\eta_{-1}}{\tan(\varpi)}\right) e^{i\Xi}, \tag{4.21}$$

where $\varpi = ax - (am\mu + c\lambda\, p)y + ct, \quad \Xi = mx + (a^2\mu + c^2\lambda - \frac{1}{2}\, \lambda\, p^2 - \frac{1}{2}\, m^2\mu)y + pt + q.$

Case. B.2

$$\begin{aligned} &\eta_0 = 0, \eta_1 = \eta_1, \eta_{-1} = 0, a = a, c = c, m = m, q = q, \lambda = \lambda, \\ &n = a^2\mu + c^2\lambda - \frac{1}{2}\, \lambda\, p^2 - \frac{1}{2}\, m^2\mu, \mu = \mu, \nu = \frac{a^2\mu + c^2\lambda}{{\eta_1}^2}. \end{aligned} \tag{4.22}$$

Thus, the subsequent optical soliton solution is produced:

$$z_{B,2,1}(x, y, t) = \left(\eta_1 \tan(\varpi)\right) e^{i\Xi}, \tag{4.23}$$

where $\varpi = ax - (am\mu + c\lambda\, p)y + ct, \quad \Xi = mx + (a^2\mu + c^2\lambda - \frac{1}{2}\,\lambda\, p^2 - \frac{1}{2}\, m^2\mu)y + pt + q.$

Case. B.3

$$\begin{aligned} &\eta_0 = 0, \eta_1 = \eta_{-1}, \eta_{-1} = \eta_{-1}, a = a, c = c, m = m, q = q, \lambda = \lambda, \\ &n = -2\, a^2\mu - 2\, c^2\lambda - \frac{1}{2}\,\lambda\, p^2 - \frac{1}{2}\, m^2\mu, \mu = \mu, \nu = \frac{a^2\mu + c^2\lambda}{{\eta_{-1}}^2}. \end{aligned} \tag{4.24}$$

Thus, the subsequent optical soliton solution is produced:

$$z_{B,3,1}(x, y, t) = \left(\frac{\eta_{-1}}{\tan(\varpi)} + \eta_{-1}\tan(\varpi)\right)e^{i\Xi}, \tag{4.25}$$

where $\varpi = ax - (am\mu + c\lambda\, p)y + ct, \quad \Xi = mx + (-2\, a^2\mu - 2\, c^2\lambda - \frac{1}{2}\,\lambda\, p^2 - \frac{1}{2}\, m^2\mu)y + pt + q.$

Case. B.4

$$\begin{aligned} &\eta_0 = 0, \eta_1 = -\eta_{-1}, \eta_{-1} = \eta_{-1}, a = a, c = c, m = m, q = q, \lambda = \lambda, \\ &n = 4\, a^2\mu + 4\, c^2\lambda - \frac{1}{2}\,\lambda\, p^2 - \frac{1}{2}\, m^2\mu, \mu = \mu, \nu = \frac{a^2\mu + c^2\lambda}{{\eta_{-1}}^2}. \end{aligned} \tag{4.26}$$

Thus, the subsequent optical soliton solution is produced:

$$z_{B,4,1}(x, y, t) = \left(\frac{\eta_{-1}}{\tan(\varpi)} - \eta_{-1}\tan(\varpi)\right)e^{i\Xi}, \tag{4.27}$$

where $\varpi = ax - (am\mu + c\lambda\, p)y + ct, \quad \Xi = mx + (4\, a^2\mu + 4\, c^2\lambda - \frac{1}{2}\,\lambda\, p^2 - \frac{1}{2}\, m^2\mu)y + pt + q.$

4.3. The application of tanh-coth method

We finally apply the tanh-coth method to (2.3) in order to provide novel soliton solutions for (2.1). The proposed tanh-coth method presents the following close-form solution for (2.3) when $\Omega = 1$ is substituted in (3.6):

$$Z(\varpi) = \sum_{r=-1}^{1} \eta_r\,(\tanh(\varpi))^r\,. \tag{4.28}$$

When incorporated in (2.3), this solution further converts the NODE into an expression in $\tanh(\varpi)$. By collecting and equating the coefficients with the same powers of $\tanh(\varpi)$ to zero, we get a system of algebraic equations. By running the resultant system through computational tool Maple, we get the following cases of solutions for the system:

Case. C.1

$$\begin{aligned} &\eta_0 = 0, \eta_1 = 0, \eta_{-1} = \eta_{-1}, a = a, c = c, m = m, q = q, \lambda = \lambda, \\ &n = -a^2\mu - c^2\lambda - \frac{1}{2}\,\lambda\, p^2 - \frac{1}{2}\, m^2\mu, \mu = \mu, \nu = \frac{a^2\mu + c^2\lambda}{{\eta_{-1}}^2}. \end{aligned} \tag{4.29}$$

Thus, the subsequent optical soliton solution is produced:

$$z_{C,1,1}(x, y, t) = \left(\frac{\eta_{-1}}{\tanh(\varpi)}\right)e^{i\Xi}, \tag{4.30}$$

where $\varpi = ax - (am\mu + c\lambda\, p)y + ct, \quad \Xi = mx + (-a^2\mu - c^2\lambda - \frac{1}{2}\,\lambda\, p^2 - \frac{1}{2}\, m^2\mu)y + pt + q.$

Case. C.2

$$\begin{aligned} &\eta_0 = 0, \eta_1 = \eta_1, \eta_{-1} = 0, a = a, c = c, m = m, q = q, \lambda = \lambda, \\ &n = -a^2\mu - c^2\lambda - \frac{1}{2}\,\lambda\, p^2 - \frac{1}{2}\, m^2\mu, \mu = \mu, \nu = \frac{a^2\mu + c^2\lambda}{{\eta_1}^2}. \end{aligned} \tag{4.31}$$

Thus, the subsequent optical soliton solution is produced:

$$z_{C,2,1}(x, y, t) = \Big(\eta_1 \tanh(\varpi)\Big)e^{i\Xi}, \tag{4.32}$$

where $\varpi = ax - (am\mu + c\lambda\, p)y + ct, \quad \Xi = mx + (-a^2\mu - c^2\lambda - \frac{1}{2}\,\lambda\, p^2 - \frac{1}{2}\, m^2\mu)y + pt + q.$

Case. C.3

$$\begin{aligned} &\eta_0 = 0, \eta_1 = \eta_{-1}, \eta_{-1} = \eta_{-1}, a = a, c = c, m = m, q = q, \lambda = \lambda, \\ &n = -4\, a^2\mu - 4\, c^2\lambda - \frac{1}{2}\,\lambda\, p^2 - \frac{1}{2}\, m^2\mu, \mu = \mu, \nu = \frac{a^2\mu + c^2\lambda}{{\eta_{-1}}^2}. \end{aligned} \tag{4.33}$$

Thus, the subsequent optical soliton solution is produced:

$$z_{C,3,1}(x, y, t) = \Big(\frac{\eta_{-1}}{\tanh(\varpi)} + \eta_{-1} \tanh(\varpi)\Big)e^{i\Xi}. \tag{4.34}$$

where $\varpi = ax - (am\mu + c\lambda\, p)y + ct, \quad \Xi = mx + (-4\, a^2\mu - 4\, c^2\lambda - \frac{1}{2}\,\lambda\, p^2 - \frac{1}{2}\, m^2\mu)y + pt + q.$

Case. C.4

$$\begin{aligned} &\eta_0 = 0, \eta_1 = -\eta_{-1}, \eta_{-1} = \eta_{-1}, a = a, c = c, m = m, q = q, \lambda = \lambda, \\ &n = 2\, a^2\mu + 2\, c^2\lambda - \frac{1}{2}\,\lambda\, p^2 - \frac{1}{2}\, m^2\mu, \mu = \mu, \nu = \frac{a^2\mu + c^2\lambda}{{\eta_{-1}}^2}. \end{aligned} \tag{4.35}$$

Thus, the subsequent optical soliton solution is produced:

$$z_{C,4,1}(x, y, t) = \Big(\frac{\eta_{-1}}{\tanh(\varpi)} - \eta_{-1} \tanh(\varpi)\Big)e^{i\Xi}, \tag{4.36}$$

where $\varpi = ax - (am\mu + c\lambda\, p)y + ct, \quad \Xi = mx + (2\, a^2\mu + 2\, c^2\lambda - \frac{1}{2}\,\lambda\, p^2 - \frac{1}{2}\, m^2\mu)y + pt + q.$

5. Graphical analysis

This section graphically illustrates and examines the propagation dynamics of the obtained optical soliton solutions of the desired model. In the context of the chosen NPWE, the optical soliton solutions were developed based on the proposed methods. Along with smooth, singular, periodic, and breather interaction solutions in the form of trigonometric, hyperbolic, and Jacobian elliptic functions, we obtained dark and bright solutions. A set of 2D and 3D graphs illustrates the dynamics and interaction of the generated optical soliton solutions for the numerical values of the free parameters. We further clarify that some parameters are free parameters, which can take any value, while some parameters are dependent parameters determined by constraint relation from the process of solution.

Breather interaction is a dynamical structure where two or more breather solitons coexist and interact, leading to fusions, oscillatory exchanges of energy or collisions. In optical fibers or nonlinear media, this corresponds to interacting pulses or beams, where energy can transfer between modes but overall structure is preserved. The superposition and nonlinear interaction of breather modes cause temporary constructive and destructive interference patterns. We also revealed some other type of breather solitons such as singular breather, smooth breather, and periodic breather solitons. A singular breather soliton develops sharp spikes or has localized singularities in amplitude during the oscillation that occurs when the focusing nonlinearity overpowers dispersion locally, producing points of extreme amplitude in the wave solution.

In optical fields, singular breathers correspond to intensity spikes, which may signal instability or collapse phenomena in beam propagation. A smooth breather soliton is a localized wave packet whose amplitude oscillates periodically in the propagation direction but remains smooth and bounded. This breather type represents a pulse or beam in nonlinear optics that periodically breathes in width and intensity but does not lose energy, analogous to a laser pulse that periodically compresses and broadens during propagation and arises from interference between dispersive spreading and nonlinear self-focusing when the complex field evolves out of phase.

Periodic breather solitons appear due to resonance between the nonlinear term and the effective dispersion relation of the system and is a breather solution whose oscillations in amplitude repeat periodically in the transverse direction and propagation direction. The periodic modulation can be seen as a standing breather pattern. In optics, periodic breathers are useful for modeling optical frequency combs or modulated pulse propagation and represent modulated beams or pulse trains that self-repeat.

From the squared norms of the solutions, we get two types of soliton structures: dark and bight solitons. A dark soliton is a localized dip in a continuous-wave background, with intensity approaching a finite constant at infinity that appears in the defocusing regime, where nonlinear effects cause a notch in the otherwise uniform background. In optics, dark solitons correspond to intensity depressions in a broad continuous-wave laser beam, often with a phase jump across the dip. A bright soliton is a localized, hump-shaped intensity profile that decays to zero at infinity. The squared norm removes oscillations of real and imaginary parts of the solutions, leaving a smooth intensity hump. This soliton type represents a localized optical pulse or beam of high intensity traveling without spreading.

In Figure 8, **A., D.** real part and **B., E.** imaginary part represent smooth breather solitons while **C., F.** squared norm represents bell-shaped dark soliton in the context of optical soliton solution $z_{A,1,2}(x, y, t)$ stated in (4.5) to the (2+1)-dimensional NPWE with parameters $s = 0.99998, \rho = \frac{1}{4}, \varrho = \frac{-2s^2+1}{2}, \sigma = \frac{1}{4}, a = 0.01, c = 0.03, m = 0.05, p = 0.015, q = 0, \lambda = 0.01, \mu = 0.02, \eta_{-1} = 1$.

In Figure 9, **A., D.** real part and **B., E.** imaginary part represent singular breather solitons, while **C., F.** squared norm represents dark soliton in the context of optical solitons solution $z_{A,1,5}(x, y, t)$ stated in (4.7) to the (2+1)-dimensional NPWE with parameters $s = 0.999, \rho = 1, \varrho = -s^2 + 2, \sigma = -s^2 + 1, a = 0.5, c = 0.01, m = 0.4, p = 0.5, q = 1, \lambda = 0.2, \mu = 0.03, \eta_{-1} = 2$.

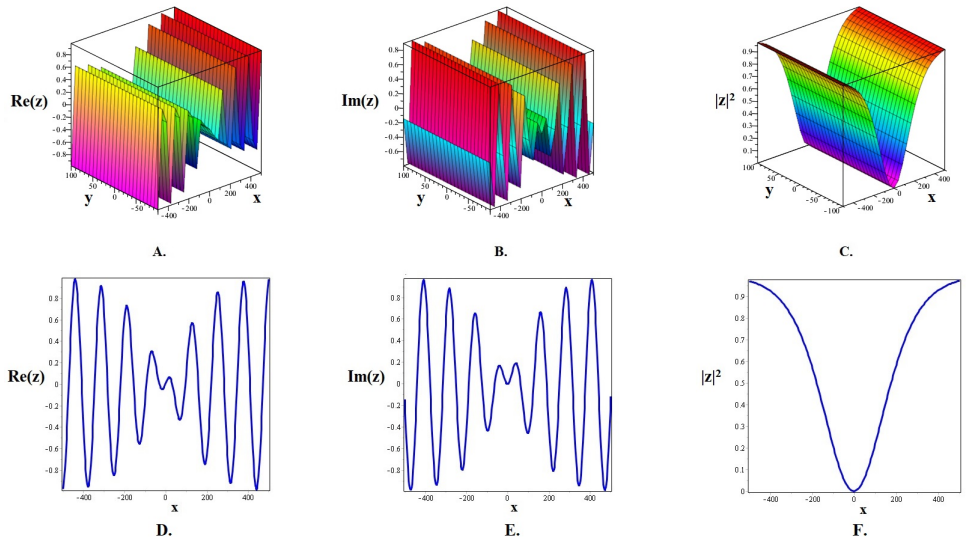

Figure 8. The 3D and 2D (when $y = 10$) depictions of the real part $Re(z)$, imaginary part $Im(z)$ and squared norm $|z|^2$ of the optical soliton solution $z_{A,1,2}(x, y, t)$ stated in (4.5) to the (2+1)-dimensional NPWE with parameter values $s = 0.99998, \rho = \frac{1}{4}, \varrho = \frac{-2s^2+1}{2}, \sigma = \frac{1}{4}, a = 0.01, c = 0.03, m = 0.05, p = 0.015, q = 0, \lambda = 0.01, \mu = 0.02, \eta_{-1} = 1, t = 1$.

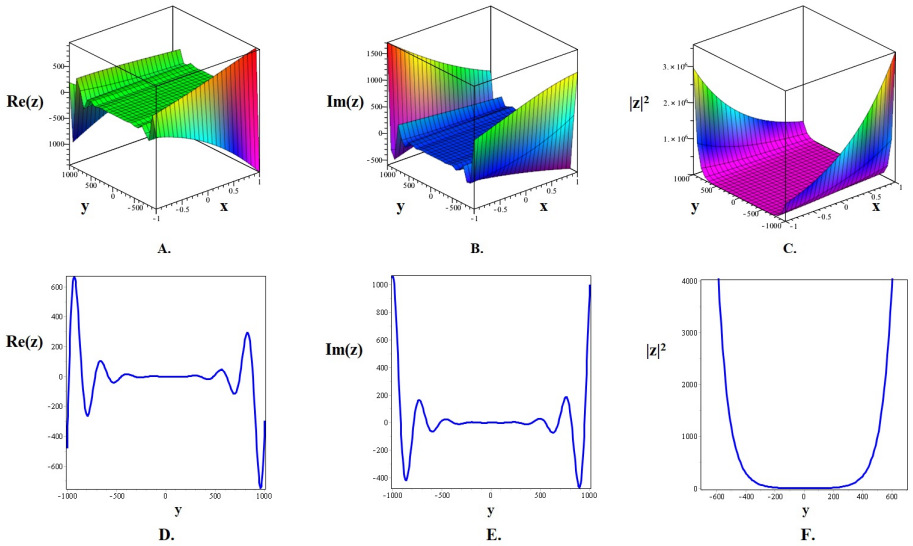

Figure 9. The 3D and 2D (when $x = 0$) depictions of the real part $Re(z)$, imaginary part $Im(z)$, and squared norm $|z|^2$ of the optical soliton solution $z_{A,1,5}(x, y, t)$ stated in (4.7) to the (2+1)-dimensional NPWE with parameter values $s = 0.999, \rho = 1, \varrho = -s^2 + 2, \sigma = -s^2 + 1, a = 0.5, c = 0.01, m = 0.4, p = 0.5, q = 1, \lambda = 0.2, \mu = 0.03, \eta_{-1} = 2, t = 5$.

In Figure 10, **A., D.** real part and **B., E.** imaginary part represent singular breather solitons, while **C., F.** squared norm represents periodic dark-bright soliton in the context of optical soliton solution $z_{A,1,11}(x, y, t)$ stated in (4.13) to the (2+1)-dimensional NPWE with parameters $s = 0.001, \rho = \frac{1}{4}, \varrho = \frac{-2s^2+1}{2}, \sigma = \frac{1}{4}, a = 0.1, c = 0.02, m = 0.5, p = 0.1, q = 0, \lambda = 0.1, \mu = 0.05, \eta_{-1} = 5$. In Figure 11,

A., D. real part and **B., E.** imaginary part reveal the formation of internal envelope solitons due to the breather interaction while **C., F.** squared norm represents bright solitons in the context of optical soliton solution $z_{A,1,12}(x, y, t)$ stated in (4.14) to the (2+1)-dimensional NPWE with parameters $s = 0.0005, \rho = \frac{-s^2+1}{4}, \varrho = \frac{s^2+1}{2}, \sigma = \frac{-s^2+1}{4}, a = 0.001, c = 0.02, m = 0.04, p = 0.03, q = 0.1, \lambda = 0.4, \mu = 0.5, \eta_{-1} = 1$.

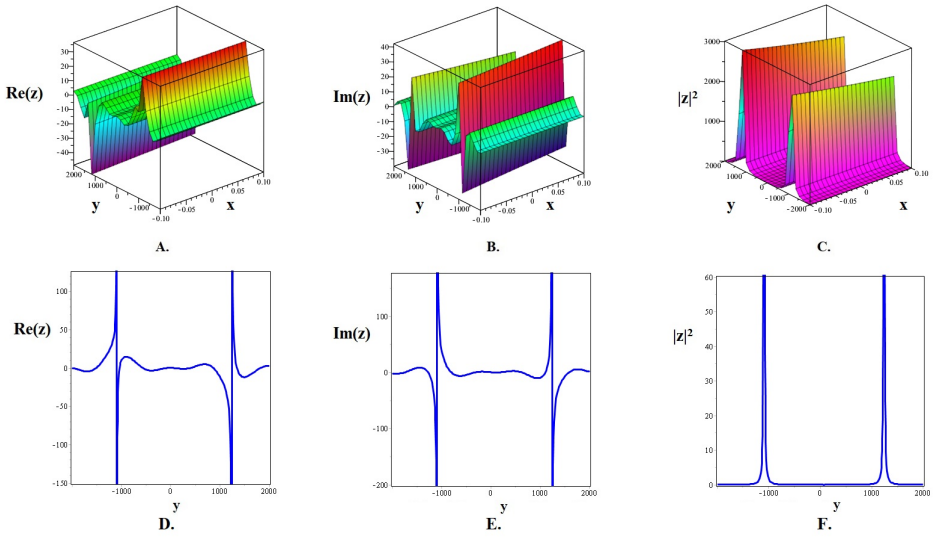

Figure 10. The 3D and 2D (when $x = 0$) depictions of the real part $Re(z)$, imaginary part $Im(z)$, and squared norm $|z|^2$ of the optical soliton solution $z_{A,1,11}(x, y, t)$ stated in (4.13) to the (2+1)-dimensional NPWE with parameter values $s = 0.001, \rho = \frac{1}{4}, \varrho = \frac{-2s^2+1}{2}, \sigma = \frac{1}{4}, a = 0.1, c = 0.02, m = 0.5, p = 0.1, q = 0, \lambda = 0.1, \mu = 0.05, \eta_{-1} = 5, t = 10$.

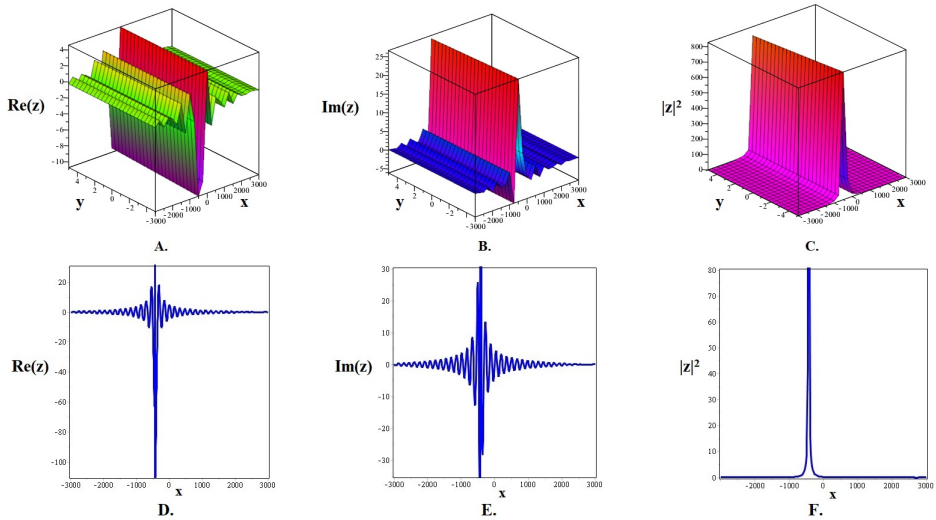

Figure 11. The 3D and 2D (when $y = 5$) depictions of the real part $Re(z)$, imaginary part $Im(z)$, and squared norm $|z|^2$ of the optical soliton solution $z_{A,1,12}(x, y, t)$ stated in (4.14) to the (2+1)-dimensional NPWE with parameter values $s = 0.0005, \rho = \frac{-s^2+1}{4}, \varrho = \frac{s^2+1}{2}, \sigma = \frac{-s^2+1}{4}, a = 0.001, c = 0.02, m = 0.04, p = 0.03, q = 0.1, \lambda = 0.4, \mu = 0.5, \eta_{-1} = 1, t = 100$.

In Figure 12, **A., D.** real part and **B., E.** imaginary part reveal breather interaction, while **C., F.** squared norm represents periodic dark solitons in the context of optical soliton solution $z_{B,2,1}(x, y, t)$ stated in (4.23) to the (2+1)-dimensional NPWE with parameters $a = 0.3, c = 0.1, m = 0.0045, p = 0.005, q = 0.1, \lambda = 0.005, \mu = 0.01, \eta_1 = 2$. In Figure 13, **A., D.** real part and **B., E.** imaginary part represent periodic breather, while **C., F.** squared norm represents bell-shaped dark solitons in the context of optical soliton solution $z_{C,2,1}(x, y, t)$ stated in (4.30) to the (2+1)-dimensional NPWE with parameters $a = 0.003, c = 0.05, m = 0.01, p = 0.05, q = 0.9, \lambda = 0.4, \mu = 0.5, \eta_1 = 3$.

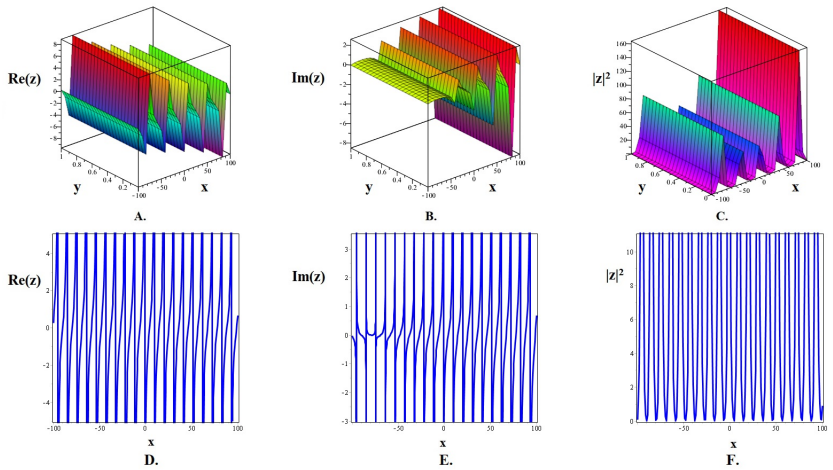

Figure 12. The 3D and 2D (when $y = 1$) depictions of the real part $Re(z)$, imaginary part $Im(z)$ and squared norm $|z|^2$, of the optical soliton solution $z_{B,2,1}(x, y, t)$ stated in (4.23) to the (2+1)-dimensional NPWE with parameter values $a = 0.3, c = 0.1, m = 0.0045, p = 0.005, q = 0.1, \lambda = 0.005, \mu = 0.01, \eta_1 = 2, t = 50$.

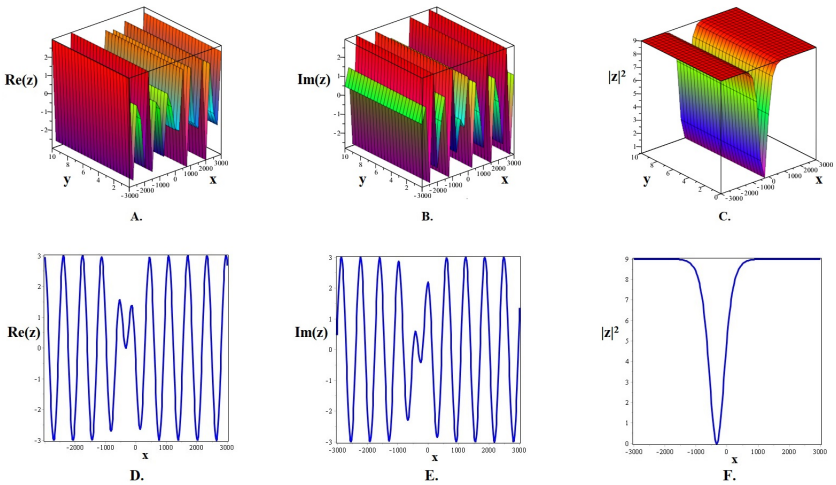

Figure 13. The 3D and 2D (when $y = 10$) depictions of the real part $Re(z)$, imaginary part $Im(z)$, and squared norm $|z|^2$ of the optical soliton solution $z_{C,2,1}(x, y, t)$ stated in (4.30) to the (2+1)-dimensional NPWE with parameter values $a = 0.003, c = 0.05, m = 0.01, p = 0.05, q = 0.9, \lambda = 0.4, \mu = 0.5, \eta_1 = 3, t = 20$.

Finally, the Figure 14, **A., D.** real part and **B., E.** imaginary part reveal singular, lump-like breather, while **C., F.** squared norm represents bright solitons in the context of optical soliton solution $z_{C,4,1}(x, y, t)$ stated in (56) to the (2+1)-dimensional NPWE with parameter $a = 0.005, c = 0.009, m = 0.005, p = 0.001, q = 0, \lambda = 0.001, \mu = 0.003, \eta_{-1} = 5$.

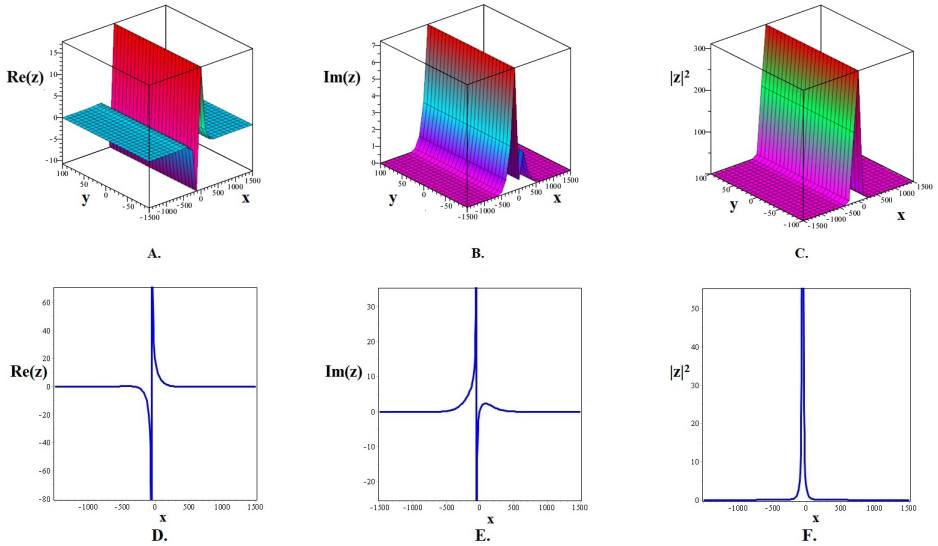

Figure 14. The 3D and 2D (when $y = 100$) depictions of the real part $Re(z)$, imaginary part $Im(z)$, and squared norm $|z|^2$ of the optical solitons solution $z_{C,4,1}(x, y, t)$ stated in (4.32) to the (2+1)-dimensional NPWE with parameters values $a = 0.005, c = 0.009, m = 0.005, p = 0.001, q = 0, \lambda = 0.001, \mu = 0.003, \eta_{-1} = 5, t = 30$.

6. Novelties, comparative analysis, and limitations

No other work has produced optical soliton solutions for NPWE with dynamical analysis of the model via phase portraits and time series plots utilizing the suggested GKAM, tan-cot approach, and tanh-coth method in the literature. This claim draws attention to a substantial gap in the corpus of recent research. By using the recommended techniques and providing a comprehensive model analysis, our study closes this gap. To more clearly identify how the system is susceptible to perturbation, we also undertake dynamical analysis to evaluate the flexibility the chosen model against the variations of the parameters and initial conditions. The acquired results are important for fiber optics, nonlinear optics, and communication systems. Besides assessing the soliton phenomena in the stated NPWE, the suggested work confirms the efficiency of the recommended methods by determining the formation of the soliton solutions of various models in nonlinear settings. The presented approaches that yield closed-form solutions were selected because, like other methods, they do not require complicated operations such as perturbation, linearization, discretization, and so forth. when dealing with nonlinear models. The methods proposed are innovative and efficient because they provide many explicit solutions in the form of Jacobian elliptic, hyperbolic, and trigonometric functions. Such solutions provide a deeper knowledge of the underlying process of the models since it makes consideration of a broad range of wave patterns; which other methods would overlook or fail to measure. However, it is crucial to acknowledge the limitations of the proposed approaches , such as

the fact that the proposed methods fail when the homogeneous balancing principle cannot balance the nonlinear term with the highest derivative term in order to provide soliton solutions.

7. Conclusions

Optical soliton solutions to the complex-structured NPWE have been examined in this research study through three ansatzes, namely the GKAM, the tan-cot method, and the tanh-coth method. The recommended methods were used to find breather and other optical soliton solutions of the selected NPWE, including dark and bright solutions, smooth, singular, periodic, and breather-interaction solutions in the form of trigonometric, hyperbolic, and Jacobian elliptic functions. We have also shown a set of 2D and 3D graphs that depicted the dynamics and interaction of the constructed optical soliton solutions for the numerical values of the free parameters. Dynamical analysis of the selected model was also performed to see the flexibility of the model to the variation in the parameters and initial conditions so that the sensitiveness of the system in chaos can be understood better. The outcomes obtained are very important in fiber optics, nonlinear optics, and communication systems. Furthermore, the approaches taken provided soliton solutions of NPDEs explicitly, and this could help to understand better the phenomena of nonlinear waves and provide new hints into the dynamics of other complex systems.

Future goal: The future ambitions of this research study will be aimed at conducting stability analysis of soliton solutions and studying the suggested model in both fractional and stochastic senses using several analytical approaches.

Use of Generative-AI tools declaration

The author declares he has not used Artificial Intelligence (AI) tools in the creation of this article.

Acknowledgments

The author is thankful to the Deanship of Graduate Studies and Scientific Research at the University of Bisha for supporting this work through the Fast-Track Research Support Program.

References

1. A. W. Leung, Systems of nonlinear partial differential equations: Applications to biology and engineering, Springer Dordrecht, 1989. https://doi.org/10.1007/978-94-015-3937-1
2. P. H. Rabinowitz, Some minimax theorems and applications to nonlinear partial differential equations, In: *Nonlinear analysis*, 1978, 161–177. https://doi.org/10.1016/B978-0-12-165550-1.50016-1
3. S. Malik, M. S. Hashemi, S. Kumar, H. Rezazadeh, W. Mahmoud, M. S. Osman, Application of new Kudryashov method to various nonlinear partial differential equations. *Opt. Quant. Electron.*, **55** (2023), 8. https://doi.org/10.1007/s11082-022-04261-y
4. A. W. Leung, *Nonlinear systems of partial differential equations: Applications to life and physical sciences*, World Scientific, 2009. https://doi.org/ 10.1142/7353

5. T. A. Nofal, Simple equation method for nonlinear partial differential equations and its applications, *J. Egyptian Math. Soc.*, **24**, (2016), 204–209. https://doi.org/10.1016/j.joems.2015.05.006
6. S. N. Antontsev, J. Diaz, S. Shmarev, A. Kassab, Energy methods for free boundary problems: Applications to nonlinear PDEs and fluid mechanics. Progress in nonlinear differential equations and their applications, *Appl. Mech. Rev.*, **55** (2002), B74–B75. https://doi.org/10.1115/1.1483358
7. L. Debnath, *Nonlinear partial differential equations for scientists and engineers*, *Boston: Birkhäuser*, 2005.
8. H. Chen, X. Tao, B. Zhu, J. Pan, L. Ma, C. Chen, et al., Reconfigurable nonlinear Pancharatnam-Berry diffractive optics with photopatterned ferroelectric nematics, *Light Sci. Appl.*, **14** (2025), 314. https://doi.org/10.1038/s41377-025-01981-0
9. X. Guo, J. Zhang, X. Meng, Z. Li, X. Wen, P. Girard, et al., HALTRAV: Design of a high-performance and area-efficient latch with triple-node-upset recovery and algorithm-based verifications, *IEEE T. Comput.-Aid. D.*, **44** (2025), 2367–2377. https://doi.org/10.1109/TCAD.2024.3511335
10. S. A. El-Tantawy, H. A. Alyousef, R. T. Matoog, R. Shah, On the optical soliton solutions to the fractional complex structured (1+1)-dimensional perturbed Gerdjikov-Ivanov equation, *Phys. Scr.*, **99** (2024), 035249. https://doi.org/10.1088/1402-4896/ad241b
11. S. Noor, A. S. Alshehry, A. Shafee, R. Shah, Families of propagating soliton solutions for (3+1)-fractional Wazwaz-BenjaminBona-Mahony equation through a novel modification of modified extended direct algebraic method, *Phys. Scr.*, **99**, (2024), 045230. https://doi.org/10.1088/1402-4896/ad23b0
12. N. Iqbal, W. W. Mohammed, A. E. Hamza, S. Hussain, Y. Jawarneh, R. Shah, Fractals and chaotic solitons phenomena in conformable coupled higgs system, *Discrete Dyn. Nat. Soc.*, **1**, (2025), 8384630. https://doi.org/10.1155/ddns/8384630
13. N. Iqbal, S. Mukhtar, A. M. Saeed, R. Shah, S. Hussain, New solitary and soliton wave solutions of the fractional Higgs system using a Riccati-Bernoulli and Bäcklund framework, *Nonlinear Dyn.*, **113** (2025), 26505–26519. https://doi.org/10.1007/s11071-025-11430-7
14. W. Alhejaili, R. Shah, A. H. Salas, S. Raut, S. Roy, A. Roy, et al., Unearthing the existence of intermode soliton-like solutions within integrable quintic Kundu–Eckhaus equation, *Rend. Lincei. Sci. Fis.*, **36** (2025), 233–255. https://doi.org/10.1007/s12210-024-01288-z
15. Y. He, M. Yuan, Q. Li, L. Tang, W. Yang, Y. Ping, et al., Feasibility study of mechanical stress wave detection in power semiconductor devices using bare FBG sensors, *IEEE Sens. J.*, **25** (2025), 39849–39857. https://doi.org/10.1109/JSEN.2025.3615108
16. Z. Chen, L. Zhong, X. Sun, Y. Fu, H. He, H. Ji, et al., 25 nm-Feature, 104-aspect-ratio, 10-mm2-area single-pulsed laser nanolithography, *Nat. Commun.*, **16** (2025), 7434. https://doi.org/10.1038/s41467-025-62426-1
17. D. Saha, P. Chatterjee, S. Raut, Multi-shock and soliton solutions of the Burgers equation employing Darboux transformation with the help of the Lax pair, *Pramana*, **97** (2023), 54. https://doi.org/10.1007/s12043-023-02534-z
18. S. Kumar, B. Mohan, A study of multi-soliton solutions, breather, lumps, and their interactions for kadomtsev-petviashvili equation with variable time coeffcient using hirota method, *Phys. Scr.*, **96** (2021), 125255. https://doi.org/10.1088/1402-4896/ac3879

19. M. Tahir, A. U. Awan, K. A. Abro, Extraction of optical solitons in birefringent fibers for Biswas-Arshed equation via extended trial equation method, *Nonlinear Eng.*, **10** (2021), 146–158. https://doi.org/10.1515/nleng-2021-0011
20. V. E. Zakharov, The inverse scattering method, In: *Solitons*, Berlin Heidelberg: Springer, 1980, 243–285. https://doi.org/10.1007/978-3-642-81448-8_7
21. Y. Xiao, S. Barak, M. Hleili, K. Shah, Exploring the dynamical behaviour of optical solitons in integrable kairat-II and kairat-X equations, *Phys. Scr.*, **99** (2024), 095261. https://doi.org/10.1088/1402-4896/ad6e34
22. E. Tala-Tebue, Z. I. Djoufack, S. B. Yamgoué, A. Kenfack-Jiotsa, T. C. Kofané, New soliton solutions for a discrete electrical lattice using the Jacobi elliptical function method. *Chinese J. Phys.*, **56** (2018), 1010–1020. https://doi.org/10.1016/j.cjph.2018.03.027
23. A. Zulfiqar, J. Ahmad, Soliton solutions of fractional modified unstable Schrödinger equation using Exp-function method, *Results Phys.*, **19** (2020), 103476. https://doi.org/10.1016/j.rinp.2020.103476
24. Z. Rahman, M. Z. Ali, H. O. Roshid, Closed form soliton solutions of three nonlinear fractional models through proposed improved Kudryashov method, *Chinese Phys. B*, **30** (2021), 050202. https://doi.org/10.1088/1674-1056/abd165
25. R. Ali, M. M. Alam, S. Barak, Exploring chaotic behavior of optical solitons in complex structured conformable perturbed Radhakrishnan-Kundu-Lakshmanan model, *Phys. Scr.*, **99** (2024), 095209. https://doi.org/10.1088/1402-4896/ad67b1
26. E. Yusufoğlu, A. Bekir, Solitons and periodic solutions of coupled nonlinear evolution equations by using the sine–cosine method, *Int. J. Comput. Math.*, **83** (2006), 915–924. https://doi.org/10.1080/00207160601138756
27. K. R. Raslan, The first integral method for solving some important nonlinear partial differential equations, *Nonlinear Dyn,*, **53** (2008), 281–286. https://doi.org/10.1007/s11071-007-9262-x
28. A. Rani, A. Zulfiqar, J. Ahmad, Q. M. Ul Hassan, New soliton wave structures of fractional Gilson-Pickering equation using tanh-coth method and their applications, *Results Phys.*, **29** (2021), 104724. https://doi.org/10.1016/j.rinp.2021.104724
29. M. Mirzazadeh, Soliton solutions of Davey–Stewartson equation by trial equation method and ansatz approach, *Nonlinear Dyn.*, **82**, (2015), 1775–1780. https://doi.org/10.1007/S11071-015-2276-X
30. H. Yasmin, N. H. Aljahdaly, A. M. Saeed, R. Shah, Probing families of optical soliton solutions in fractional perturbed Radhakrishnan–Kundu–Lakshmanan model with improved versions of extended direct algebraic method, *Fractal Fract.*, **7** (2023), 512. https://doi.org/10.3390/fractalfract7070512
31. M. M. Islam, M. Ahbab, M. R. Islam, M. H. Kabir, On the exact soliton solutions of some nonlinear PDE by Tan-Cot method. *GUB J. Sci. Eng.*, **5** (2018), 31–36. https://doi.org/10.3329/gubjse.v5i1.47898
32. R. Ali, Z. Zhang, H. Ahmad, M. M. Alam, The analytical study of soliton dynamics in fractional coupled Higgs system using the generalized Khater method, *Opt. Quant. Electron.*, **56** (2024), 1067. https://doi.org/10.1007/s11082-024-06924-4

33. H. H. Hussein, H. M. Ahmed, W. Alexan, Analytical soliton solutions for cubic-quartic perturbations of the Lakshmanan-Porsezian-Daniel equation using the modified extended tanh function method, *Ain Shams Eng. J.*, **15** (2024), 102513. https://doi.org/10.1016/j.asej.2023.102513
34. M. M. Roshid, M. M. Rahman, H. O. Roshid, M. H. Bashar, A variety of soliton solutions of time M-fractional: Non-linear models via a unified technique, *Plos One*, **19** (2024), 0300321. https://doi.org/10.1371/journal.pone.0300321
35. H. A. Alyousef, R. Shah, A. H. Salas, C. G. L. Tiofack, S. M. Ismaeel, W. Alhejaili, et al., On the solitons, shocks, and periodic wave solutions to the fractional quintic Benney–Lin equation for liquid film dynamics, *Math. Method. Appl. Sci.*, **48** (2025), 6145–6164. https://doi.org/10.1002/mma.10661
36. M. Arshad, A. R. Seadawy, D. Lu, F. U. Khan, Optical solitons of the paraxial wave dynamical model in Kerr media and its applications in nonlinear optics, *Int. J. Mod. Phys. B*, **34** (2020), 2050078. https://doi.org/10.1142/S0217979220500782
37. A. Djazet, S. I. Fewo, E. B. Ngompe Nkouankam, T. C. Kofane, Stability analysis for moving dissipative solitons in two-dimensional dynamical model, *Eur. Phys.l J. D*, **74** (2020), 67. https://doi.org/10.1140/epjd/e2020-100467-7
38. M. H. Bashar, M. A. Mannaf, M. M. Rahman, M. T. Khatun, Optical soliton solutions of the M-fractional paraxial wave equation, *Sci. Rep.*, **15** (2025), 1416. https://doi.org/10.1038/s41598-024-74323-6
39. F. Baronio, S. Wabnitz, Y. Kodama, Optical Kerr spatiotemporal dark-lump dynamics of hydrodynamic origin, *Phys. Rev. Lett.*, **116** (2016), 173901. https://doi.org/10.1103/PhysRevLett.116.173901
40. M. Arshad, A. R. Seadawy, D. Lu, M. S. Saleem, Elliptic function solutions, modulation instability and optical solitons analysis of the paraxial wave dynamical model with Kerr media, *Opt. Quant. Electron.*, **53** (2021), 7. https://doi.org/10.1007/s11082-020-02637-6
41. U. Younas, J. Muhammad, H. F. Ismael, T. A. Sulaiman, H. Emadifar, K. K. Ahmed, Diversity of solitary wave structures in Kerr media: Analyzing the complex paraxial wave equation in fiber optic communication systems, *Ain Shams Eng. J.*, **16** (2025), 103763. https://doi.org/10.1016/j.asej.2025.103763
42. B. S. T. Alkahtani, Retrieval of lump, breather, interactions, and rogue wave solutions to the fractional complex paraxial wave dynamical model with sensitivity analysis, *Opt. Mater. Express*, **14** (2024), 2431–2450. https://doi.org/10.1364/OME.534962
43. K. L. Wang, C. F. Wei, Novel optical soliton solutions to nonlinear paraxial wave model, *Modern Phys. Lett. B*, **39** (2025), 2450469. https://doi.org/10.1142/S0217984924504694